A DSC and XPS characterization of Core-shell Morphology of Block Copolymer Nanoparticles

Vitalii Tkachenko, Ludovic Josien, Gautier Schrodj, Samar Hajjar-Garreau, Sébastien Urbaniak, Julien Poly, Abraham Chemtob

A DSC and XPS characterization of Core-shell Morphology of Block Copolymer Nanoparticles

Vitalii Tkachenko,[1,2] Ludovic Josien,[1,2] Gautier Schrodj,[1,2] Samar Hajjar-Garreau,[1,2] Sébastien Urbaniak,[3] Julien Poly[1,2*] and Abraham Chemtob[1,2*]

[1] Université de Haute-Alsace, CNRS, IS2M UMR7361, F-68100 Mulhouse, France

[2] Université de Strasbourg, France

[3] Université Claude Bernard Lyon 1, CNRS, LAGEPP UMR5007, F-69622 Villeurbanne, France

*Corresponding author : e-mail (abraham.chemtob@uha.fr), tel (+33 3 8960 8834), Orcid Number (0000-0003-4434-1870)

Abstract

Self-assembly of amphiphilic block copolymer chains is known to produce core-shell nanoparticles, but imaging techniques have generally failed to provide clear evidence about the multiphase structure. We report herein the advantages and limitations of modulated temperature differential scanning calorimetry (MDSC) and X-ray photoelectron spectroscopy (XPS) for the morphology study of spherical poly(hydroxyethyl acrylate)-b-polystyrene diblock copolymer nanoparticles with an intensity average-diameter of 40 nm. Using lyophilized particles, MDSC is more informative than XPS since it allows the three morphological features of composite latex particles to be distinguished: polystyrene core, poly(hydroxyethyl acrylate) shell and interface. In MDSC, phase separation is evidenced by two distinct increments of heat capacity (ΔCp) in the glass transitions regions of the two blocks. By measuring ΔCp values, an interface weight fraction of 70% is measured that gradually decreases to 50% with annealing time (150 °C, 2 h), indicating a higher extent of phase separation.

Keywords

Copolymers, Dispersions, Self-assembly, Modulated differential scanning calorimetry, Particle morphology, Structured latex, X-ray photoelectron spectroscopy

Introduction

Core-shell latexes are part of structured composite particles. They feature at least two separate bulk polymer phases of different chemical composition preferentially located on particle surface and at the center [1]. Such latex architecture with two spatially separated components has attracted interest in a variety of applications, some of them characterized by high tonnage productions, such as impact modifiers, waterborne coatings and adhesives [2]. Core-shell latex particles are typically synthesized by interfacial polymerization in dispersed media, in which a shell-forming monomer is polymerized by emulsion polymerization on the surface of seeded "core" particles [3]. The typical core-shell latex particle that results from this method contains two polymeric phases composed of two distinct homopolymers or random copolymers [4]. In addition to the two-step method, other variant methods have been described in the literature [1], as well as more complex particle architectures including raspberry-, confetti- or sandwich-type [5]. Generation of two separate polymer domains within the confined space of a core-shell particle is driven by the interplay of thermodynamic factors (interfacial tension of polymer phases, reaction temperature, cross-linking, etc.) and kinetic factors (initiator type and concentration, feeding rate of the shell-forming monomer, etc.). To evidence the multiphase structure of composite latex particle, mostly imaging techniques such as transmission electron microscopy (TEM) [6], or in less extent, atomic force microscopy (AFM) [7] are typically used [8]. Other non-microscopic techniques such as dynamic scanning calorimetry (DSC) [9] or solid-state NMR [10] have been employed to obtain indirectly some data on the quantitative fraction for the various phases.

Recently, a new class of core-shell nanoparticles based on amphiphilic graft or block copolymers has emerged [11]. They consist of a solvophobic polymer core coated with a solvophilic stabilizing polymer shell. In contrast to conventional core-shell particles, the two polymer components are covalently bonded and the particles can be accessed via single-step polymerization methods without the need of external surfactant. The preferred synthesis method is based on self-assembly of amphiphilic block copolymers such as polymerization-induced self-assembly (PISA) [12], but other techniques also exist such as free radical copolymerization of hydrophilic macromonomers with hydrophobic monomers [13] or graft copolymerizations from water-soluble macroinitiators [14]. The applications for these particles are also different, including diagnostic testing, bio-separations, controlled release of drugs and other biological agents [15]. Unlike the first type of core-shell particles, characterizing the multiphase structure of these self-assembled core-shell particles is generally very challenging. In a few isolated studies only [16–19], TEM has provided indisputable evidences of the core-shell morphology through the contrasted observation of multiple polymeric domains within the particle. However, in a majority of studies, usage of electron microscopy is made difficult by particle sizes smaller than 100 nm. In addition, the low glass transition temperature of the shell component leads to particles highly susceptible to structural changes upon drying or exposure to radiation of electrons [20].

In the quest for alternative solutions, we report herein the advantages and limitations of two analytical techniques for the morphology study of core-shell amphiphilic diblock copolymer nanoparticles: DSC and X-ray photoelectron spectroscopy (XPS). The spherical particles were prepared by visible-light photo-PISA in

dispersion in which a soft solvophilic poly(hydroxyethyl acrylate) (PHEA, T_g = -7.3°C, degree of polymerization = 85) homopolymer is chain extended with a hard solvophobic polystyrene (PS, T_g = 99.0°C, degree of polymerization = 130) via a photomediated reversible-addition–fragmentation-transfer (RAFT) polymerization. The resulting $PHEA_{85}$-b-PS_{130} particles have an intensity average-diameter of 40 nm (dynamic light scattering data) and their typical core-shell structure is sketched in **Fig. 1**.

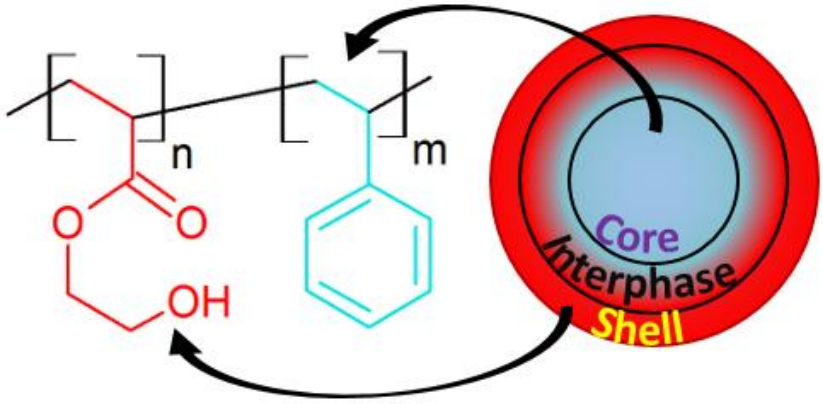

Fig. 1. Schematic representation of a poly(hydroxyethyl acrylate)-*b*-polystyrene ($PHEA_{85}$-*b*-PS_{130}) core−shell nanoparticle. It features a hydrophobic core made up of PS and palisade composed by PHEA block segments. The interphase is the intermediate zone between the two bulk regions

- In DSC, the change in heat capacity for each block segment (PHEA or PS) across the T_g can be used to determine the amount of bulk polymer phase. Therefore, DSC is able to determine quantitatively the weight fractions of PS in the core and PHEA in the shell, the remainder corresponding to the interface. This latter can be defined as a region of finite thickness within which the composition varies continuously from one bulk phase to the other. Note that an interfacial region is formed within the particle even when the two polymer segments forming the block copolymer are incompatible, because of the interdiffusion of a fraction of the two copolymer phases [21–23]. DSC has already proved to be a valuable technique to study the core-shell morphology of 2-component polymer particles produced by seeded emulsion polymerization [8, 24, 25], but never with amphiphilic copolymer nanoparticles. Originally reported by Tembu-Nzudie et al. in 1994 for poly(butadiene)/poly(methyl methacrylate) latex [26], the method was further elaborated [24]. In particular, the groups of Hourston [27, 28], Karlsson [29, 30], and Sunberg [31, 32] have emphasized the interest of DSC or modulated temperature DSC for determining the interfacial content of composite latex.

- XPS has a typical analysis depth of less than 7 nm. Therefore, only the latex “surface” is likely to be probed, thus shedding light into the shell composition. Given its sensitivity to atomic composition, XPS could thus distinguish the solvophilic PHEA from the solvophobic PS block because it is the only block containing oxygen atoms. XPS has previously been used to quantitatively assess the surface composition of polymeric particles [33], and recently the morphology nanoparticles of poly(styrene)/poly(methyl methacrylate) core-shell latex [34]. The presence of a surface stabilizer [35] and the efficiency of particle surface modification were also studied by XPS [36].

Experimental section

Materials

For a typical synthesis of $PHEA_{85}$-*b*-PS_{130} block copolymer based nanoparticles, $PHEA_{85}$-TTC (TTC: – S-cyanomethyl-S-dodecyltrithiocarbonate) (0.838 g, 0.083 mmol), styrene (1.721 g, 16.528 mmol) and a methanol/water mixture (8.177 g/0.430 g, 95/5 wt/wt%) were charged into a Schlenk tube equipped with a stirring bar. The mixture was degassed by three freeze–pump–thaw cycles before being placed under nitrogen. The tube was then placed in a pre-heated oil bath at 35 °C and irradiated during 70 h in an immersion type photoreactor (λ = 472 nm, 547 mW cm^{-2}). SEC traces and DLS data are presented in Fig. S1 [37]. The copolymers nanoparticles were dispersed in methanol/water (95/5 wt/wt%) and had a solids content of 18.5 wt%. The degree of polymerization was determined by ^{1}H NMR and the molecular weights (SEC) were characterized by size exclusion chromatography (SEC) in *N*,*N*-dimethylformamide: M_n = 23.1 × 10^3 g mol^{-1}, M_w/M_n = 1.43. Analysis by dynamic light scattering (DLS) of particles showed a z-average value of 39.7 nm (conc. = 0.1 wt.%). SEC trace and DLS size distribution of $PHEA_{85}$-*b*-PS_{130} particles were provided in **Fig. S1** of ESM. PS homopolymer (M_w = 20 × 10^3 g mol^{-1}) was purchased from Fluka. Tetrahydrofuran (THF, HPLC-Isocratic grade) was obtained from Carlo Erba.

Dry copolymer samples were analyzed XPS and DSC. Three procedures were set out to dry the nanoparticles:

i. Lyophilized latex. Lyophilization is meant to preserve, as much as possible, the original core-shell morphology of the wet nanoparticles. To prepare freeze-dried nanoparticles, 6 mL vials were filled with the copolymer dispersions and placed into a freeze dryer (Cryonext, Cryotec France). The samples were frozen in the freeze dryer; the shelves being cooled at -0.5°C min^{-1}. The samples were then kept for 3 h at -40°C in order to ensure a complete freezing. Drying was performed at a pressure of 10 Pa. The temperature was first maintained at -30°C during 8 h, then -15°C for 5 h and finally 0°C for 3 h. A desorption step allowing complete drying of the sample was then applied. The samples were maintained in the freeze dryer, the temperature was set at 25°C and the pressure was increased first at 1 Pa for 12 h then at 10 Pa for 8 h.

ii. Latex film. The continuous phase of the dispersion was evaporated to create a nanostructured film. For this, the films were prepared by spreading a thin layer (0.1 to 0.3 mm) of a copolymer dispersion on a clean glass substrate or in a DSC sample pan. The latex films were left 12 h at ambient conditions to dry, and then analyzed without annealing. The film was clear and free of cracks.

iii. Solution film. The nanoparticles were dissolved in a good solvent to disrupt the self-assembly, then solvent was evaporated to create a film displaying in principle homogeneously mixed polymer blocks. For this, 5 mL of THF was added to 1 mL of copolymer dispersion to dissolve the nanoparticles. The 50 µL of homogeneous solution was cast in a DSC pan or a XPS mold. Then, the solution was dried at room temperature for 12 h.

Methods

Modulated differential scanning calorimetry (MDSC). MDSC of lyophilized copolymer nanoparticles was performed with a Mettler-Toledo DSC1. The sample was heated from -50°C to 150°C with an oscillation amplitude of 1.5°C, an oscillation period of 60 s, and a heating rate of 3°C min^{-1}. Only the data of the first scan were analyzed so that the state of mixing in the original sample was not altered by measurement. Total heat flow was separated into two components attributed to reversible and non-reversible heat flows. Only the reversible (or in-phase) component was used for the calculation of C_p and dC_p/dT. Details on the mathematical treatment of the reversible component were provided in ESM. Similar analysis was also carried after various thermal annealing times (1, 2, 5, 10, 30, and 120 min) at 150°C.

In each instance, it was possible to determine the amount of interface and bulk phases in core-shell particles from the increment of heat capacity of PHEA and PS phases across the T_g in $PHEA_{85}$-*b*-PS_{130} copolymer (ΔC_p) and in equivalent PHEA and PS homopolymers (ΔC_{p0}).

The weight fractions of PHEA in the shell (δ^s_{PHEA}) and PS in the core (δ^c_{PS}) can be expressed as follows:

$$\delta^s_{PHEA} = \omega_{PHEA} \times \left(\frac{\Delta C_p^{PHEA}}{\Delta C_{p0}^{PHEA}}\right) \quad (1)$$

$$\delta^c_{PS} = \omega_{PS} \times \left(\frac{\Delta C_p^{PS}}{\Delta C_{p0}^{PS}}\right) \quad (2)$$

Where ω_{PHEA} and ω_{PS} are respectively the weight fractions of PHEA and PS blocks in $PHEA_{85}$-*b*-PS_{130} copolymer. The values ω_{PHEA} = 0.42 and ω_{PS} = 0.59 were derived from the degrees of polymerization obtained by ^{1}H NMR data. ΔC_p^{PHEA} and ΔC_p^{PS} are increments of heat capacities for PHEA and PS in copolymer sample at glass transition temperatures, ΔC_{p0}^{PHEA} and ΔC_{p0}^{PS} are increments of heat capacities for pure PHEA and PS homopolymers. DSC traces of homopolymer shown in **Fig. S2** (ESM) give ΔC_{p0}^{PHEA} = 0.047 J g^{-1} °C^{-2} and ΔC_{p0}^{PS} = 0.054 J g^{-1} °C^{-2}.

The weight fractions of PHEA and PS in interfacial phase, δ^i_{PHEA} and δ^i_{PS} respectively, can be expressed as [27]:

$$\delta^i_{PHEA} = \omega_{PHEA} \times \left(1 - \frac{\Delta C_p^{PHEA}}{\Delta C_{p0}^{PHEA}}\right) \quad (3)$$

$$\delta^i_{PS} = \omega_{PS} \times \left(1 - \frac{\Delta C_p^{PS}}{\Delta C_{p0}^{PS}}\right) \quad (4)$$

The weight fraction of the interface can be expressed as follows:

$$W^i = \delta^i_{PHEA} + \delta^i_{PS} \quad (5)$$

Scanning Electron Microscopy (SEM). SEM was performed on a JEOL JSM-7900F microscope. In order to protect the copolymer nanoparticles, images were recorded with a 4 kV sample bias voltage and a very low accelerating voltage of 0.5 kV.

X-ray photoelectron spectroscopy (XPS). XPS experiments were performed *in situ* ($P < 10^{-9}$ mbar) with a VG Scienta SES 200-2 spectrometer using a monochromatic Al-Ka X-ray source (hv = 1468.6 eV). The Spectra were measured at normal incidence. The depth analysis is about 7 nm. The high resolution spectra and wide scan were collected with pass energy of 100 eV and 500 eV respectively. The deconvolution of the spectra into different components was performed with Gaussian (70%)—Lorentzian (30%) shaped peak using casaXPS software (version 2.3.18) after having subtracted a Shirley-type background. The atomic percent is determined using integrated peak areas of each component and taking into account the transmission factor of the spectrometer, the mean free path, and the sensibility factor of each atom.

Cryo-TEM. The vitrification of the samples was carried out in a homemade vitrification system. The chamber was held at 22°C and the relative humidity at 80%. A 5 µL drop of the sample (1–2 mg·mL^{-1}) was deposited onto a lacey carbon film covered grid (Ted Pella, Redding, CA, USA) rendered hydrophilic using an ELMO glow discharge unit (Cordouan Technologies, Bordeaux, France). The grid was automatically blotted to form a thin film which was plunged in liquid ethane held at −190 °C by liquid nitrogen. That way, a vitrified film was obtained, in which the native structure of the particles was preserved. The grid was mounted onto a cryo holder (Gatan 626, Pleasanton, CA, USA) and observed under low dose conditions in a Tecnai G2 microscope (FEI, Eindhoven, Netherland) at 200 kV. Images were acquired using an Eagle slow scan CCD camera (FEI). The number average-diameter $D_{\mathrm{n}} = \sum D_{\mathrm{TEM}}/n$ was calculated using at a minimum number of particles (*n*) of 200. The size dispersity PDI_{TEM} is the ratio of weight-average diameter D_{w} over D_{n} where $D_{\mathrm{w}} = \sum D_{\mathrm{TEM}}^4 / \sum D_{\mathrm{TEM}}^3$.

Results and Discussion

I. Cryo-TEM

Fig. 2 shows two cryo-TEM pictures at low (**a**) and high magnification (**b**) obtained from $PHEA_{85}$-*b*-PS_{130} latex. Cryo-TEM was chosen over other imaging techniques because it is recognized as the most amenable to the examination of soft nanomaterials. Indeed, the particles can be studied in their most native state without the need of specimen drying. As can be seen on the TEM image **a**, the spherical particles exhibit a narrow polydispersity index (PDI_{TEM} = 1.03) and a small apparent diameter (D_n = 21.6 ± 3.2 nm). The particles have seemingly a homogeneous structure devoid of apparent polymer domains. This result is in contrast with the common representation of a core-shell particle where both copolymer blocks are assumed to phase separate at nanoscale to form a PS core surrounded by a stabilizing PHEA palisade. A more in-depth study of the nanoparticles obtained at high magnification (image **b**) show that particles display a granular structure that was assigned to protruding PHEA chains. The stabilizing chains oriented in the z direction give rise to a higher contrast, which is manifested by black dots in the internal structure of particles. Conversely, the hydrophilic blocks arranged around the PS core (i.e. with the solvent in background) lack of contrast because they cannot adopt this specific orthogonal orientation. Unlike the PS chains aggregated in the core, the highly solvated PHEA chains cannot form dense domains and their thickness is too small to generate a contrast with the

background. Consequently, it is not possible to visualize the archetype of core-shell architecture: a corona composed of PHEA brushes surrounding a spherical PS core. In conclusion, the formation of composite particles can be evidenced by cryo-TEM, but only by expert eyes. In addition, the quantitative assessment of the size and mass distribution of the individual elements in the polymer composite has remained inaccessible by electron microscopy.

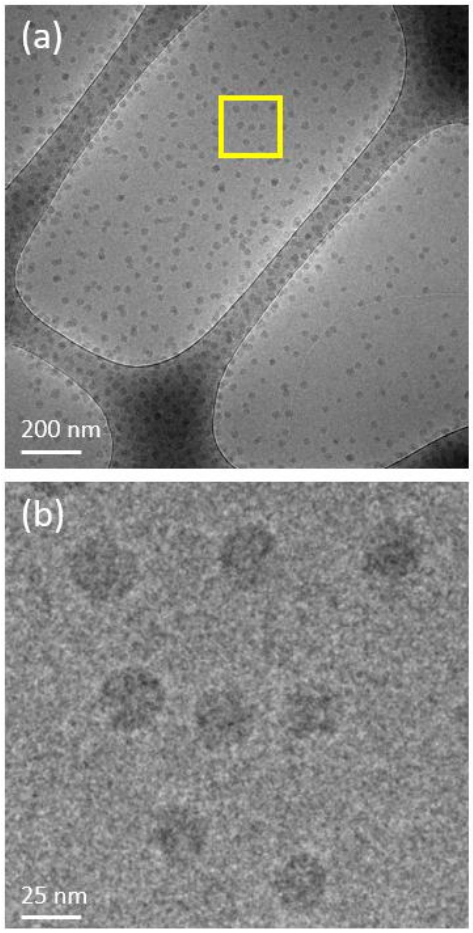

Fig. 2. (**a**) Cryo-TEM image of $PHEA_{85}$-*b*-PS_{130} latex at low magnification. (**b**) High magnification image corresponding to the framed area shown in image **a**. Concentration of copolymer dispersion = 0.1 wt.%

II. Modulated differential scanning calorimetry (MDSC)

II.1 Study of lyophilized sample by SEM

Prior to studying $PHEA_{85}$-*b*-PS_{130} block copolymer nanoparticles by DSC, the first step was to lyophilize the latex sample to maintain the integrity of the core-shell morphology (see details in the experimental conditions). Lyophilization has the dogma to preserve the core-shell architecture. However, it is not straightforward that freeze-dried structure mirrors that of the starting colloidal dispersion, in particular when particles have a soft polymer shell. In our case, dried sample are required for DSC analysis given that PS block has a glass transition of 100°C. As can be seen in **Fig. 3**, a SEM image of lyophilized particles shows that the core-shell morphology has been mostly maintained although the soft PHEA shell led to a partial coalescence of the particles boundaries.

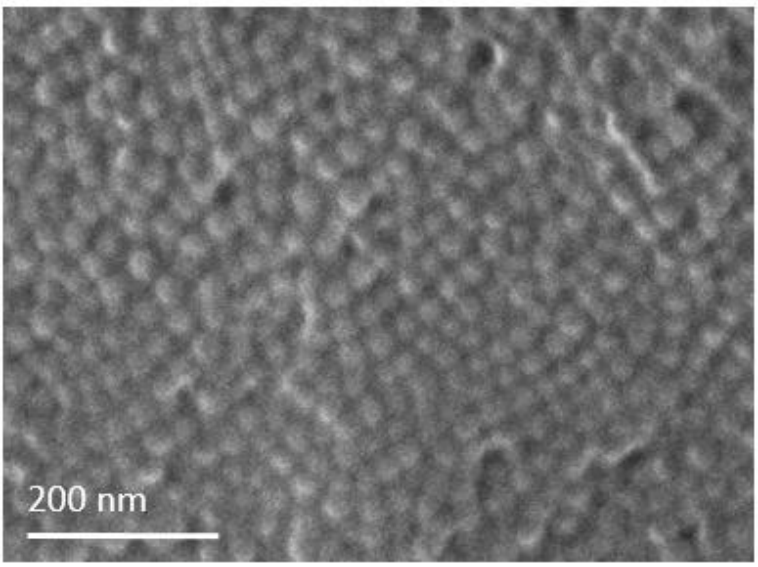

Figure 3. SEM image of lyophilized $PHEA_{85}$-*b*-PS_{130} block copolymer nanoparticles

II.2 MDSC study of lyophilized PHEA-b-PS latex

To account for the formation of distinct PS and PHEA phases within the copolymer particle, we refer to the difference of glass transition temperatures of these two blocks. Some values of respectively of -7.3°C and 99.0°C were found when analyzing by DSC $PHEA_{85}$ and PS_{130} homopolymers of similar degree of polymerization as the $PHEA_{85}$-*b*-PS_{130} block copolymer (**Fig. S2**, ESM). However, the DSC thermogram of as-lyophilized $PHEA_{85}$-*b*-PS_{130} latex shows a broad endotherm (**Fig. S3**, ESM), which makes challenging the precise assignment of the glass transition regions of PHEA and PS blocks. It is well established that conventional DSC faces problems of overlapping between thermodynamic and kinetic phenomena. To overcome this issue, modulated DSC (MDSC) has made possible to separate the total heat flow of DSC into two components: a reversible signal induced by changes in heat capacity (e.g. glass transitions) and a non-reversible signal involving only kinetic processes (enthalpic recovery and residual solvent evaporation). From the reversible signal, one can thus determine the change in heat capacity without the interference of kinetic events. **Fig. 4a** shows the variation of heat capacity (C_p) as a function of temperature data for lyophilized $PHEA_{85}$-*b*-PS_{130} nanoparticles obtained from the reversible heat flow. We took only the data of the first scan, which is the true reflection of the morphology in the original latex particle state. On the same plot are also given the results obtained from PHEA and PS homopolymers representing respectively the idealized pure shell and core phases. Although transitions can be clearly distinguished in the three heat capacity traces, it is difficult to draw conclusions due to their low intensity. To gain further information, **Fig. 4b** shows dC_p/dT, *vs.* temperature. Hourston et al. have highlighted the utility of treating DSC data in the form of temperature differential of the heat capacity as a function of temperature [27, 28]. Accordingly, the lyophilized copolymer sample (trace **1**) displays now two single and well-defined peaks at 28.1°C and 85.5°C, which can be assigned respectively to a shell phase rich in PHEA and a core phase rich in PS. The pure polymer phases of PHEA (trace **2**) and PS (trace **3**) show two intense peaks at -7.3°C and 99.0°C, in agreement with their T_g values. However, the trace of the lyophilized copolymer sample **1** is not well separated

and the broad baseline suggests a significant fraction of interfacial region. By measuring the increment of heat capacity in the two resolved glass transition regions of PHEA and PS (ΔC_{p}) and knowing the increments of pure phases (ΔC_{p0}) from traces **2** and **3**, it has been possible to determine the amount of different phases. The calculations are detailed in the experimental section. Clearly, the heat capacities $\Delta C_{\mathrm{p}}^{\mathrm{PHEA}}$ and $\Delta C_{\mathrm{p}}^{\mathrm{PS}}$ in the different copolymers are systematically lower than ΔC_{p0}. This suggests the existence of an interfacial region and the partial miscibility of the two PHEA and PS segments. It is seen that 17% of the total copolymer is in the PHEA phase (shell, δ_{PHEA}^{S}), 14% in the PS phase (core, δ_{PS}^{C}) and 69% is estimated to be the interfacial region ($W^{i} = \delta_{PS}^{i}$+δ_{PHEA}^{i}). The fraction of mixed phase is significant, but the result is not surprising given the partial miscibility of both blocks. For the PS block itself, only 24% forms a bulk core phase while 76% is entrapped in the interface. In addition, the fact that the glass transitions are shifted compared to pure polymers are indicative that the two separated phases are not pure [27–32]. The glass transitions of PHEA shell is found at 28.1°C versus – 7.3°C for the pure PHEA reference. The PS core has a transition at 85.5°C in the copolymer whereas the pure PS sample shows a sharp glass transition centered at 99.0°C. The plasticizing effect of PHEA chains trapped into PS matrix, and the rigidification induced by PS inclusion into PHEA domains account for this difference. It is another evidence of the partial miscibility of both polymers.

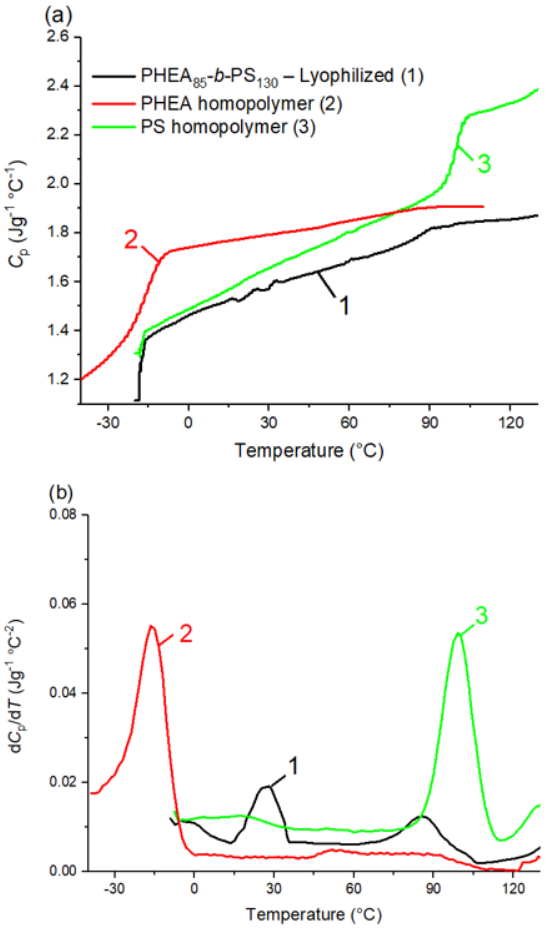

Fig. 4. (**a**) Variation of heat capacity (ΔC_{p}) as a function of temperature obtained from the reversible heat flow for lyophilized $PHEA_{85}$-*b*-PS_{130}. (**b**) Temperature differential of the heat capacity (dC_{p}/dT) as a function of temperature

II.3 Effect of annealing time on phase separation of lyophilized PHEA-b-PS latex

Because of the partial immiscibility of the core and shell phases, we speculate that phase separation in core-shell lyophilized particles could be improved upon annealing. As can be seen graphically in **Fig. 5a**, increasing time of the thermal annealing at 150°C (0 – 120 min) causes significant changes of the dC_p/dT *vs.* temperature signal. The magnitude of the dC_p/dT signals for the PHEA and PS phases increases, which suggests that the ΔC_p value also grows, and that the fractions of the pure PHEA and PS components build up. This is a clear confirmation that further and gradual phase separation takes place upon annealing. Upon thermal annealing, we can clearly see that the T_g of the PS phase rises gradually to reach after 120 min a value similar to that of the PS homopolymer. This shift translates the progressive departure of the PHEA plasticizing chains from the PS core. **Fig. 5b** shows the evolution of the weight fraction of the interface W^i (left y axis) and the total change of lost weight fraction of polymer in the interface (W^i_{lost}) as a function of annealing time. In addition, all ΔC_pvalues and weight fractions of PHEA in shell (δ^s_{PHEA}), PS core (δ^c_{PS}) and interface ($W^i = \delta^i_{\mathrm{PS}} + \delta^i_{\mathrm{PHEA}}$) were summarized in **Table 1**. W^i decreases from 69% for the as-lyophilized sample to 50% after 120 min annealing. As shown in **Table 1**, the reduction of the interfacial zone mainly results from PS chains diffusing out of the interface with time. The weight fraction of PS in the interface δ^i_{PS} thus decreases from 44% to 30% after 2 h.

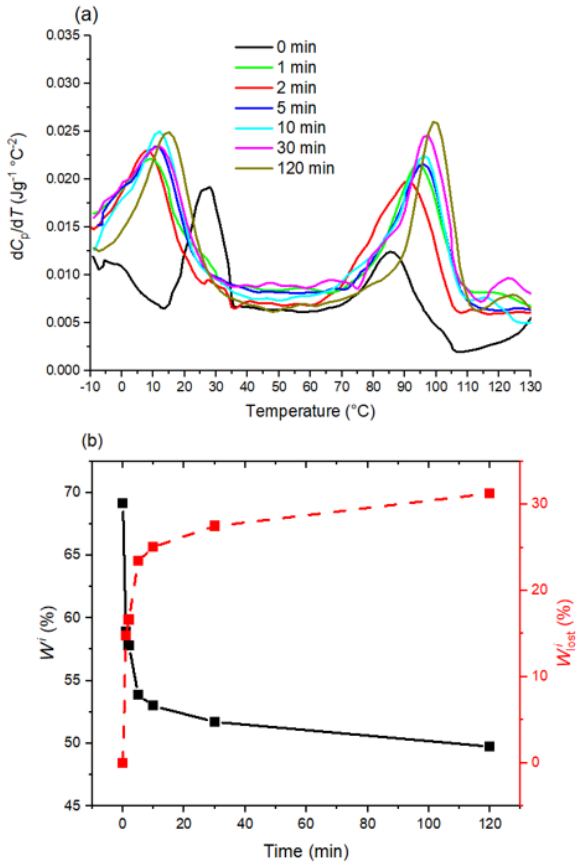

Fig. 5. (**a**) Temperature differential of the heat capacity (dC_p/dT) of core-shell lyophilized $PHEA_{85}$-*b*-PS_{130}. particles as a function of temperature for different annealing times at 150°C. (**b**) Evolution of weight fraction of the interface (solid line) and weight fraction of lost interface (dashed line) for different annealing times

Table 1. Summary data extracted from temperature differential of the heat capacity (dC_p/dT) as a function of temperature curves for lyophilized PHEA$_{85}$-*b*-PS$_{130}$ particles

Annealing time min	ΔC_p^{PHEA} J g^{-1}°C^{-2}	ΔC_p^{PS} J g^{-1}°C^{-2}	δ_{PHEA}^{i}	δ_{PS}^{i}	δ_{PHEA}^{s}	δ_{PS}^{c}	W^i %	W_{lost}^{i} %
0	0.019	0.013	0.25	0.44	0.17	0.14	69.12	0.00
1	0.022	0.02	0.22	0.37	0.19	0.22	58.90	14.79
2	0.022	0.021	0.22	0.36	0.19	0.23	57.82	16.63
5	0.024	0.023	0.20	0.34	0.21	0.25	53.88	23.43
10	0.025	0.023	0.19	0.34	0.22	0.25	53.00	25.07
30	0.024	0.025	0.20	0.31	0.21	0.27	51.72	27.48
120	0.025	0.026	0.19	0.30	0.22	0.28	49.75	31.28

ΔC_p^{PHEA} and ΔC_p^{PS} – are increments of heat capacities for PHEA and PS for current annealing time, δ_{PHEA}^{i} and δ_{PS}^{i} – are the weight fractions of PHEA and PS in the interfacial phase, δ_{PHEA}^{s} and δ_{PS}^{c} – in the corresponding pure phase, W^i – weight fraction of the interface and W_{lost}^{i} – amount of interface lost during annealing process

II.4 Effect of sample preparation

Lyophilization is the most conventional way to preserve the core-shell morphology when particles change from dispersion to dry state. To more precisely assess the impact of sample preparation on phase separation, we have changed the way the PHEA$_{85}$-*b*-PS$_{130}$ copolymer was dried. Firstly, a film was prepared from a dispersion aiming to produce a nanostructured sample by coalescence of core-shell particles. Conversely, an amorphous film where phase aggregation is minimized can be obtained from a solution where the copolymer was firstly dissolved. The preparation and the MDSC results for these two *latex* and *solution films* are described below and compared with those of the lyophilized analogue.

- **Solution film.** the copolymer was dissolved in a good solvent (THF) to disrupt the particles and a film was prepared from the solution by casting the dispersion and evaporating the continuous phase under ambient conditions. Interestingly, the dC_p/dT vs. T plot (not represented) shows no clearly defined feature which could be identified as the pure component of the copolymer. Consequently, it is not possible to reveal 2 distinct regions of PHEA and PS phases. This result suggests that in this sample the two PHEA and PS domains are intimately mixed, and that no polymer domain is formed. This is an example where the two blocks are trapped in non-equilibrium states due to kinetic restrictions. The slow diffusion of the polymer chains or/and the insufficient difference in solubility parameters of the two blocks has prevented the occurrence of a phase separation (although the precise value for both polymers is not accessible), hence no individual peaks can be identified in the DSC trace. Noteworthy is that even 2 h annealing at 150°C had no effect on this sample, and no phase segregation was observed.
- **Latex film.** To prepare this sample, the latex was cast and the continuous phase evaporated under ambient conditions as previously described. **Fig. 6a** shows the differential of heat capacity signal for different annealing times. Before treatment (t = 0), copolymer film derived from latex after solvent evaporation shows again two individual peaks related to PHEA and PS phases. However the magnitude of the dC_p/dT signals for the PS is much higher than that of PHEA. The DSC trace bears some ressemblance with that of the lyophilized sample (Fig. 5a). This result supports that a composite structure can be also preserved during latex film

formation due to the limited diffusion ability of PS chains at ambient temperature. The weight fraction of the interface of 60% is even smaller than that of lyophilized particles (69%). Similarly, the effect of annealing on W^i and W^i_{lost} is shown in **Fig. 6b**. As in the previous case, annealing caused a gradual phase separation of the core and shell components in the latex film, leading to an interface reduced to 25% after 2 h at 150°C. As can be seen in **Table 2** summarizing the weight fractions, the increase of PHEA and PS phases both account for the reduction of the interface. Lyophilized block copolymer nanoparticles have a higher initial fraction of interfacial layer (69%) comparing to air-dried film (60%) that may require a longer annealing time to achieve a phase separation comparable to that of the air-dried film.

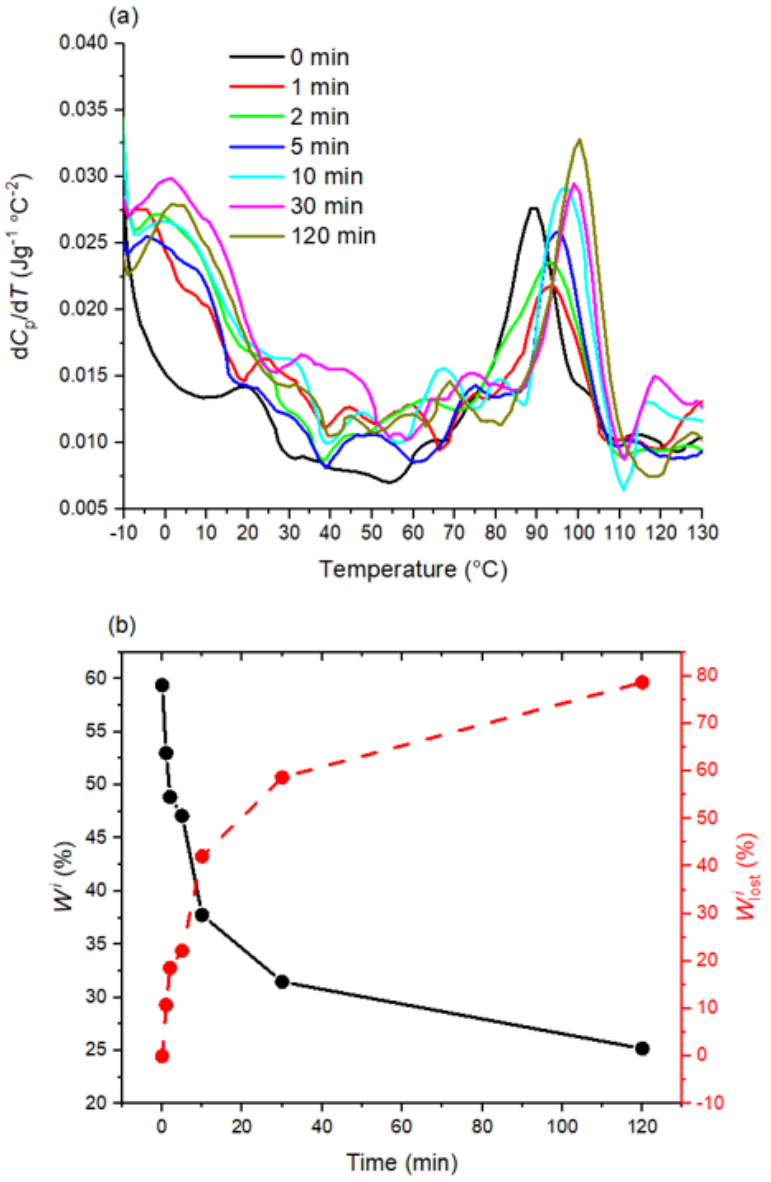

Fig. 6. (**a**) Temperature differential of the heat capacity (dC_p/dT) of latex film obtained after solvent evaporation as a function of temperature for different annealing times at 150°C for latex film obtained after solvent evaporation. (**b**) Evolution of weight fraction of the interface W^i (solid line) and weight fraction of lost interface W^i_{lost} (dashed line) for different annealing times

Table 2. Summary data extracted from temperature differential of the heat capacity (dC_p/dT) as a function of temperature curves for $PHEA_{85}$-*b*-PS_{130} latex film

Annealing time min	ΔC_p^{PHEA} J g^{-1} °C^{-2}	ΔC_p^{PS} J g^{-1} °C^{-2}	δ_{PHEA}^{i}	δ_{PS}^{i}	δ_{PHEA}^{s}	δ_{PS}^{c}	W^i %	W_{lost}^{i} %
0	0.019	0.022	0.25	0.35	0.17	0.24	59.39	0.00
1	0.025	0.023	0.19	0.34	0.22	0.25	53.00	10.77
2	0.026	0.026	0.19	0.30	0.23	0.28	48.87	18.56
5	0.028	0.026	0.17	0.30	0.25	0.28	47.10	22.19
10	0.03	0.033	0.15	0.23	0.27	0.36	37.76	42.01
30	0.031	0.038	0.14	0.17	0.27	0.41	31.47	58.67
120	0.032	0.043	0.13	0.12	0.28	0.46	25.18	78.66

III. XPS characterization

X-ray photoelectron spectroscopy (XPS) offers qualitative and quantitative data about the surface structure of particles. However, it should be noted that XPS analysis probes only the elemental and chemical composition of the particles up to approx. 7 nm in depth, which makes this method valuable only to determine the surface composition of core-shell particles [38]. Three types of $PHEA_{85}$-*b*-PS_{130} block copolymer samples were analyzed: lyophilized particles (**a**), latex film resulting from dispersion evaporation (**b**) and solution film obtained by evaporation of a THF solution (**c**). **Fig. 7** shows their XPS spectra with the surface composition of oxygen and carbon expressed as an atomic percentage (%) and determined from the integrated peak area of all elements present in a sample. In our two-component system, PS has only carbons while PHEA contains carbons and oxygen. Therefore, oxygen can act as a unique elemental marker for the PHEA phase. O1s peak but also C1s band are easily identified in the three spectra, even in the lyophilized (**a**) and nanostructured films (**b**) which are assumed to have a core-shell structure. This means that a significant amount of PS chains can be found at the surface of these two samples. Elemental analysis of lyophilized particle and nanostructured film reveal an enrichment in oxygen up to 15.01% and 15.59% compared to the theoretical value of 13.28% for $PHEA_{85}$-*b*-PS_{130} diblock copolymer (corresponding to an isotropic distribution of polymer segments). This shows that these two specific samples have a higher fraction of the PHEA solvophilic phase at their surface. By contrast, the amorphous film (**c**) has the lower content in oxygen at 9.84%, indicative of a mixed phase.

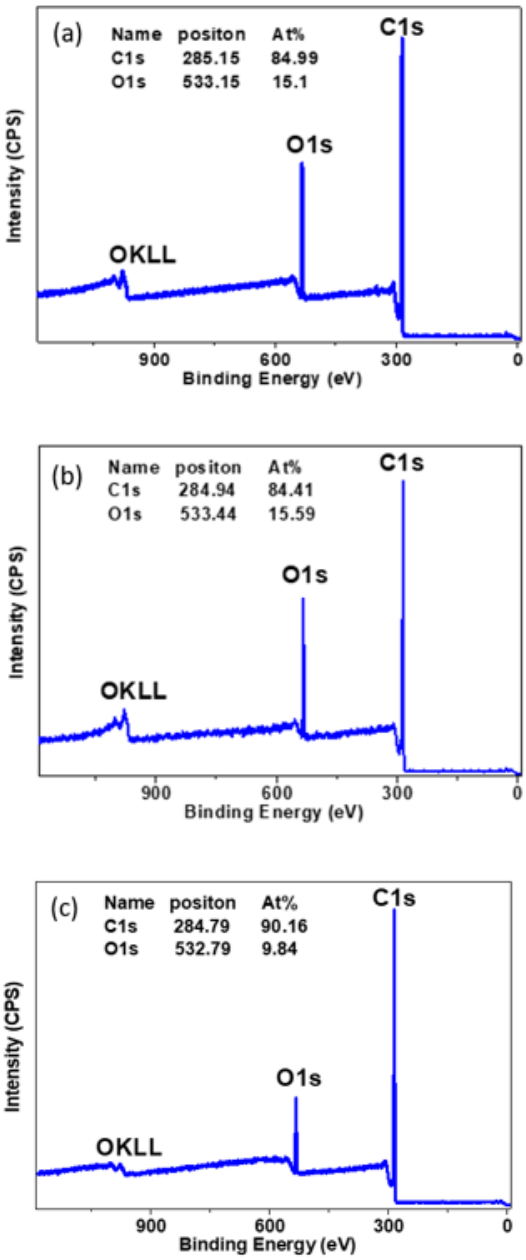

Fig. 7. XPS survey spectra of $PHEA_{85}$-*b*-PS_{130} copolymer in different forms: (**a**) lyophilized particles, (**b**) latex film and (**c**) solution films

Fig. 8 shows a high resolution analysis of the C1s peak region for the same three samples. In all instances, a fitting with five peaks was performed: the two main features were assigned to C-C and C-H (285.00 eV) and C-O (286.70 eV), and the three weak signals were attributed to O=C-O (289.5 eV), C=O (291.7 eV) and C-COO (285.4 eV). Because they are better resolved, we have paid attention to the two main resonances of C-O and C-C/CH. Both structured samples obtained by lyophilization (**a**) and latex drying (**b**) show comparable content of C-C/C-H, respectively 76.7% and 75.9%. This value is lower than theoretical value of 81.8% for a $PHEA_{85}$-*b*-PS_{130} diblock copolymer, confirming an enrichement of the surface in PHEA. The amorphous sample (**c**) with a C-C/CH signal of 81.53% agrees with an isotropic distribution of PHEA and PS phases. The integration area of the

C-O band is again similar in samples **a** and **b**, and 35 % higher than the amorphous sample **c**. However, the presence of PS remains important, and contradict the picture of a surface only occupied by PHEA chains. The first explanation relies on the diffusion of PS chains in the PHEA shell phase, which is consistent with the partial miscibility of PS in PHEA phase as proved by DSC data. Another more plaisible reason is that in the lyophilized and dried latex, the shell is strongly contracted by dehydration and the dried shell layer could have a thickness lower than 7 nm given the relatively small DP of the PHEA chain. The consequence is that not only the shell but also a part of the interface could be probed by XPS. Therefore, XPS seems less adapted than DSC to the analysis of amphiphilic copolymers nanoparticles, in particular when the spatial extent of the solvophilic shell is small. In agreement, DLS analysis revealed an intensity-average diameter of only 40 nm.

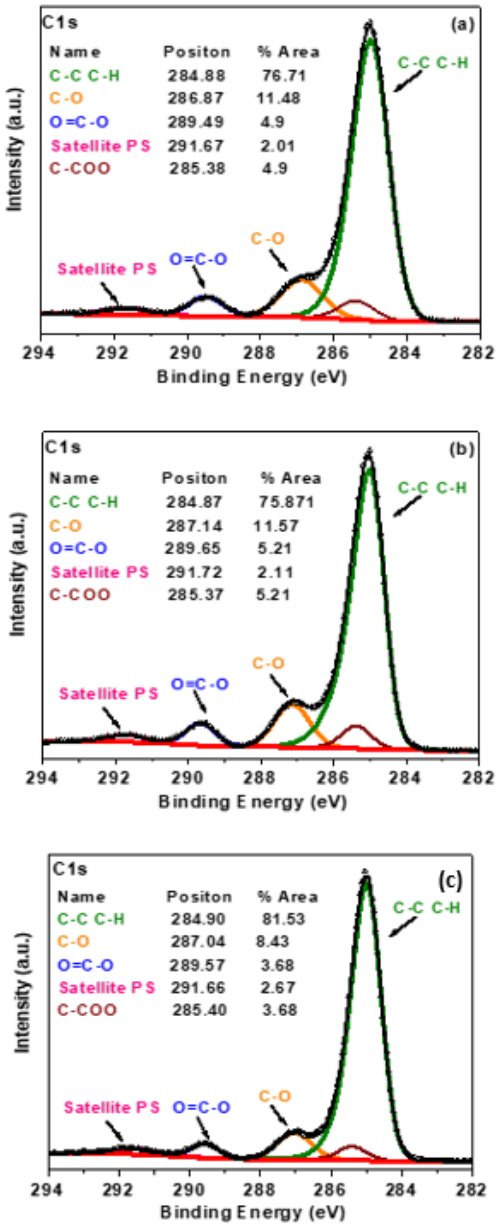

Fig. 8. C1s core-level XPS spectrum and their deconvolution for $PHEA_{85}$-*b*-PS_{130} copolymer in different forms: (**a**) lyophilized particles, (**b**) latex film and (**c**) solution films

Conclusion

The morphology of conventional core-shell particles prepared by interfacial polymerization has been extensively characterized by MDSC. In this study, we show that a similar characterization can be used for composite latex particles composed of amphiphilic block copolymers. Starting with a model $PHEA_{85}$-*b*-PS_{130} amphiphilic copolymer nanoparticles, the lyophilized sample exhibits three phase behaviors assigned to shell (PHEA), core (PS) and interface where the two blocks are homogeneously mixed. The composition of core and shell phases, the weight fraction of interface, and its evolution over annealing time can be obtained. The method can thus characterize indirectly but quantitatively the state of mixing of the two blocks within the nanoparticle while direct morphology characterization by electron microscopy can be equivocal. The method can be also exploited to investigate the extent of phase separation in the copolymer latex film after solvent evaporation, paving the way to the study of nanostructured films composed of separate polymer nanodomains.

Acknowledgements

Marc Schmutz and the electron microscopy platform at Institut Charles Sadron (CNRS, UPR 22, University of Strasbourg) are acknowledged for the cryo-TEM images and the use of the instruments.

Funding

The authors acknowledge the Ministry of Higher Education and Research in France ("Ministère de l'Enseignement Supérieur et de la Recherche", MESR) for the PhD fellowship of Vitalii Tkachenko.

Conflict of Interest

The authors declare that they have no conflict of interest.

References

1. Musyanovych A, Landfester K (2011) Core–Shell Particles. In: Macromolecular Engineering. John Wiley & Sons, Ltd, pp 1209–1247

2. Sundberg DC, Durant YG (2003) Latex Particle Morphology, Fundamental Aspects: A Review. Polymer Reaction Engineering 11:379–432. https://doi.org/10.1081/PRE-120024420

3. Ramli RA, Laftah WA, Hashim S (2013) Core–shell polymers: a review. RSC Adv 3:15543–15565. https://doi.org/10.1039/C3RA41296B

4. Ferguson CJ, Russell GT, Gilbert RG (2002) Synthesis of latices with polystyrene cores and poly(vinyl acetate) shells. 1. Use of polystyrene seeds. Polymer 43:6371–6382. https://doi.org/10.1016/S0032-3861(02)00601-8

5. Asua JM (1997) Polymeric Dispersions: Principles and Applications. Springer Netherlands

6. Wei Z, Gourevich I, Field L, et al (2006) TEM imaging of polymer multilayer particles: advantages, limitations, and artifacts. Macromolecules 39:2441–2444

7. Sommer F, Duc TM, Pirri R, et al (1995) Surface morphology of poly (butyl acrylate)/poly (methyl methacrylate) core shell latex by atomic force microscopy. Langmuir 11:440–448

8. Gosecka M, Gosecki M (2015) Characterization methods of polymer core–shell particles. Colloid Polym Sci 293:2719–2740. https://doi.org/10.1007/s00396-015-3728-z

9. Hourston DJ, Song M, Hammiche A, et al (1997) Modulated differential scanning calorimetry: 6. Thermal characterization of multicomponent polymers and interfaces. Polymer 38:1–7. https://doi.org/10.1016/S0032-3861(96)00466-1

10. Landfester K, Spiess HW (1998) Characterization of interphases in core—shell latexes by solid-state NMR. Acta Polymerica 49:451–464. https://doi.org/10.1002/(SICI)1521-4044(199809)49:9<451::AID-APOL451>3.0.CO;2-U

11. Panday R, Poudel AJ, Li X, et al (2018) Amphiphilic core-shell nanoparticles: Synthesis, biophysical properties, and applications. Colloids and Surfaces B: Biointerfaces 172:68–81. https://doi.org/10.1016/j.colsurfb.2018.08.019

12. Le D, Keller D, Delaittre G (2019) Reactive and Functional Nanoobjects by Polymerization-Induced Self-Assembly. Macromolecular Rapid Communications 40:1800551. https://doi.org/10.1002/marc.201800551

13. Búcsi A, Forcada J, Gibanel S, et al (1998) Monodisperse Polystyrene Latex Particles Functionalized by the Macromonomer Technique. Macromolecules 31:2087–2097. https://doi.org/10.1021/ma971434q

14. Li P, Zhu J, Sunintaboon P, Harris FW (2002) New Route to Amphiphilic Core−Shell Polymer Nanospheres: Graft Copolymerization of Methyl Methacrylate from Water-Soluble Polymer Chains Containing Amino Groups. Langmuir 18:8641–8646. https://doi.org/10.1021/la0261343

15. Xiong X-B, Falamarzian A, Garg SM, Lavasanifar A (2011) Engineering of amphiphilic block copolymers for polymeric micellar drug and gene delivery. Journal of Controlled Release 155:248–261. https://doi.org/10.1016/j.jconrel.2011.04.028

16. Fenyves R, Schmutz M, Horner IJ, et al (2014) Aqueous Self-Assembly of Giant Bottlebrush Block Copolymer Surfactants as Shape-Tunable Building Blocks. J Am Chem Soc 136:7762–7770. https://doi.org/10.1021/ja503283r

17. Zhu J, Tang A, Law LP, et al (2005) Amphiphilic Core−Shell Nanoparticles with Poly(ethylenimine) Shells as Potential Gene Delivery Carriers. Bioconjugate Chem 16:139–146. https://doi.org/10.1021/bc049895l

18. Gröschel AH, Müller AHE (2015) Self-assembly concepts for multicompartment nanostructures. Nanoscale 7:11841–11876. https://doi.org/10.1039/C5NR02448J

19. Müllner M, Müller AHE (2016) Cylindrical polymer brushes – Anisotropic building blocks, unimolecular templates and particulate nanocarriers. Polymer 98:389–401. https://doi.org/10.1016/j.polymer.2016.03.076

20. Franken LE, Boekema EJ, Stuart MCA (2017) Transmission Electron Microscopy as a Tool for the Characterization of Soft Materials: Application and Interpretation. Adv Sci (Weinh) 4:. https://doi.org/10.1002/advs.201600476

21. Fan X, Liu J, Jia X, et al (2017) A series of nanoparticles with phase-separated structures by 1,1-diphenylethene controlled one-step soap-free emulsion copolymerization and their application in drug release. Nano Res 10:2905–2922. https://doi.org/10.1007/s12274-017-1492-8

22. Spontak RJ, Ryan JJ (2020) Polymer blend compatibilization by the addition of block copolymers. In: Compatibilization of Polymer Blends. Elsevier, pp 57–102

23. Li N, Panagiotopoulos AZ, Nikoubashman A (2017) Structured Nanoparticles from the Self-Assembly of Polymer Blends through Rapid Solvent Exchange. Langmuir 33:6021–6028. https://doi.org/10.1021/acs.langmuir.7b00291

24. Duan M, Qiu T, Huang C, et al (2013) Synthesis of poly(acrylate-styrene)/poly(acrylate-styrene) core/shell latex and TOPEM-DSC characterization. Progress in Organic Coatings 76:216–223. https://doi.org/10.1016/j.porgcoat.2012.09.019

25. Song M, Liao B (2004) A modulated DSC characterization of morphology of composite latex particles. Thermochimica Acta 423:57–61. https://doi.org/10.1016/j.tca.2004.04.025

26. Nzudie DT, Delmotte L, Riess G (1994) Polybutadiene-poly(methyl methacrylate) core-shell latexes studied by high-resolution solid-state 13C NMR and DSC: Influence of the surface coverage of the polybutadiene seed latex and the latex composition on the interphase formation. Macromolecular Chemistry and Physics 195:2723–2737. https://doi.org/10.1002/macp.1994.021950804

27. Hourston DJ, Zhang HX, Song M, et al (1997) Modulated differential scanning calorimetry — VII: Interfacial macromolecular diffusion in core-shell latex particles. Thermochimica Acta 294:23–31. https://doi.org/10.1016/S0040-6031(96)03138-3

28. Hourston DJ, Song M (2006) Applications of Modulated Temperature Differential Scanning Calorimetry to Polymer Blends and Related Systems. In: Reading M, Hourston DJ (eds) Modulated Temperature Differential Scanning Calorimetry: Theoretical and Practical Applications in Polymer Characterisation. Springer Netherlands, Dordrecht, pp 161–215

29. Colombini D, Ljungberg N, Hassander H, Karlsson OJ (2005) The effect of the polymerization route on the amount of interphase in structured latex particles and their corresponding films. Polymer 46:1295–1308. https://doi.org/10.1016/j.polymer.2004.11.056

30. Karlsson OJ, Hassander H, Colombini D (2003) The effect of first-stage polymer Tg on the morphology and thermomechanical properties of structured polymer latex particles. Comptes Rendus Chimie 6:1233–1244. https://doi.org/10.1016/j.crci.2003.07.012

31. Stubbs JM, Sundberg DC (2005) Measuring the extent of phase separation during polymerization of composite latex particles using modulated temperature DSC. Journal of Polymer Science Part B: Polymer Physics 43:2790–2806. https://doi.org/10.1002/polb.20558

32. Tripathi AK, Tsavalas JG, Sundberg DC (2013) Quantitative measurements of the extent of phase separation during and after polymerization in polymer composites using DSC. Thermochimica Acta 568:20–30. https://doi.org/10.1016/j.tca.2013.06.013

33. Khan MA, Armes SP, Perruchot C, et al (2000) Surface Characterization of Poly(3,4-ethylenedioxythiophene)-Coated Latexes by X-ray Photoelectron Spectroscopy. Langmuir 16:4171–4179. https://doi.org/10.1021/la991390+

34. Jasinski F, Teo VL, Kuchel RP, et al (2017) Synthesis and characterisation of gradient polymeric nanoparticles. Polym Chem 8:495–499. https://doi.org/10.1039/C6PY02062C

35. Barthet C, Armes SP, Chehimi MM, et al (1998) Surface Characterization of Polyaniline-Coated Polystyrene Latexes. Langmuir 14:5032–5038. https://doi.org/10.1021/la980102r

36. Gosecka M, Griffete N, Mangeney C, et al (2011) Preparation and optical properties of novel bioactive photonic crystals obtained from core-shell poly(styrene/α-tert-butoxy-ω-vinylbenzyl-polyglycidol) microspheres. Colloid Polym Sci 289:1511–1518. https://doi.org/10.1007/s00396-011-2447-3

37. Tkachenko V, Ghimbeu CM, Vaulot C, et al (2019) RAFT-photomediated PISA in dispersion: mechanism, optical properties and application in templated synthesis. Polym Chem 10:2316–2326. https://doi.org/10.1039/C9PY00209J

38. Cairns DB, Armes SP, Chehimi MM, et al (1999) X-ray Photoelectron Spectroscopy Characterization of Submicrometer-Sized Polypyrrole−Polystyrene Composites. Langmuir 15:8059–8066. https://doi.org/10.1021/la990443k